

Article

A Fast-Response Red Shifted Fluorescent Probe for Detection of H₂S in Living Cells

Ismail Ismail ¹ , Zhuoyue Chen ², Xiuru Ji ³, Lu Sun ³, Long Yi ^{2,4,*} and Zhen Xi ^{1,4,*}

¹ State Key Laboratory of Elemento–Organic Chemistry and Department of Chemical Biology, National Engineering Research Center of Pesticide (Tianjin), College of Chemistry, Nankai University, Tianjin 300071, China; ismailics86@gmail.com

² Beijing Key Laboratory of Bioprocess and College of Chemical Engineering, Beijing University of Chemical Technology, 15 Beisanhuan East Road, Chaoyang District, Beijing 100029, China; 2018210060@mail.buct.edu.cn

³ Tianjin Key Laboratory on Technologies Enabling Development of Clinical Therapeutics and Diagnostics (Theranostics), School of Pharmacy, Tianjin Medical University, Tianjin 300070, China; jxry1217@tmu.edu.cn (X.J.); sunlu@tmu.edu.cn (L.S.)

⁴ Collaborative Innovation Center of Chemical Science and Engineering (Tianjin), Tianjin 300071, China

* Correspondence: yilong@mail.buct.edu.cn (L.Y.); zhenxi@nankai.edu.cn (Z.X.); Tel.: +86 022-23504782 (Z.X.); Fax: +86 022-23500952 (Z.X.)

Academic Editor: Maged Henary

Received: 11 November 2019; Accepted: 27 December 2019; Published: 21 January 2020



Abstract: Near-infrared (NIR) fluorescent probes are attractive tools for bioimaging applications because of their low auto-fluorescence interference, minimal damage to living samples, and deep tissue penetration. H₂S is a gaseous signaling molecule that is involved in redox homeostasis and numerous biological processes in vivo. To this end, we have developed a new red shifted fluorescent probe **1** to detect physiological H₂S in live cells. The probe **1** is based on a rhodamine derivative as the red shifted fluorophore and the thiolysis of 7-nitro 1,2,3-benzoxadiazole (NBD) amine as the H₂S receptor. The probe **1** displays fast fluorescent enhancement at 660 nm (about 10-fold turn-ons, $k_2 = 29.8 \text{ M}^{-1}\text{s}^{-1}$) after reacting with H₂S in buffer (pH 7.4), and the fluorescence quantum yield of the activated red shifted product can reach 0.29. The probe **1** also exhibits high selectivity and sensitivity towards H₂S. Moreover, **1** is cell-membrane-permeable and mitochondria-targeting, and can be used for imaging of endogenous H₂S in living cells. We believe that this red shifted fluorescent probe can be a useful tool for studies of H₂S biology.

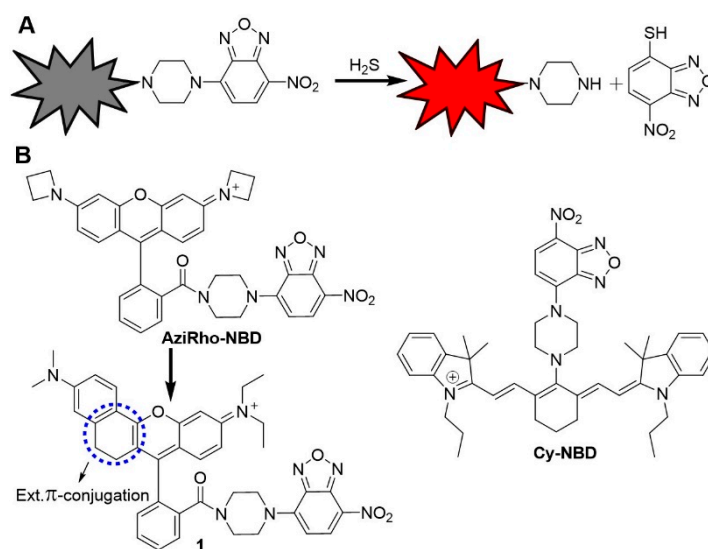
Keywords: fluorescent probe; red shifted; H₂S; bioimaging

1. Introduction

Recently biological reports have demonstrated the important role of H₂S, and the results suggested that endogenously-produced hydrogen sulfide (H₂S) has been marked as gasotransmitter, allowing the regulation of numerous important physiological functions including; cardiovascular, gastrointestinal, endocrine, nervous, and immune systems [1–3]. Generally, endogenous H₂S can be produced enzymatically from L-cysteine (Cys) by means of three distinctive enzymatic pathways; cystathionine γ -lyase (CSE), cystathionine β -synthetase (CBS), and 3-mercaptopyruvate sulfurtransferase (3-MST) [4]. The interest in the molecular mechanisms of H₂S associated with physiology and pathology was sparked out of its recognition as a vital signaling molecule. However, the abnormal levels of H₂S production lead to number of different human diseases including; diabetes [5], Alzheimer’s disease [6] liver cirrhosis [7], and the symptoms of Down’s syndrome [8–10]. As an important role played by H₂S in tumor biology, it is proposed that the both production and inhibition of H₂S concentration beyond a

threshold level could exert anticancer effects [10,11]. While in plants, the growth and development, seed germination, and stress tolerance including cross-adaptation are regulated by H₂S [12–14]. H₂S also plays important role in microorganisms [15]. Due to its wide distribution in all organisms, the physiological characters of H₂S and the precise mechanisms by which H₂S may involve in vivo still remain largely unexplored. Therefore, adequate tools (H₂S probes or donors) are necessary to further explore H₂S biology [16–21]. For cellular H₂S detection, various fluorescence probes have been successfully developed [22–38]. However, H₂S fluorescence probes for in vivo bioimaging are still rare [16–18], especially for the imaging of H₂S-related diseases including cancers [22]. Due to the potential limitations of fluorescent probes in deep tissue penetration, photodamage to biological samples, and background auto-fluorescence in living systems, it is crucial to develop probes associated with long wavelength emission especially in the red shifted region [39–42].

Recently, numbers of red shifted and NIR fluorescent dyes have been developed [43–51]. Consequently, various NIR fluorescent probes have been designed on the basis of different organic reaction scenario [8,52–58]. Among them, we as well as others discovered a reaction of H₂S-specific thiolysis of 7-nitro 1,2,3-benzoxadiazole (NBD) amines [33,58,59] to detect millimolar H₂S in a long range wavelength. Herein, this reaction strategy is further employed for the development of a new red shifted fluorescent probe 1 (Scheme 1).



Scheme 1. (A) The thiolysis of 7-nitro 1,2,3-benzoxadiazole (NBD) amine reaction for H₂S fluorescence probe. (B) Chemical structures of selected NBD-based H₂S probes.

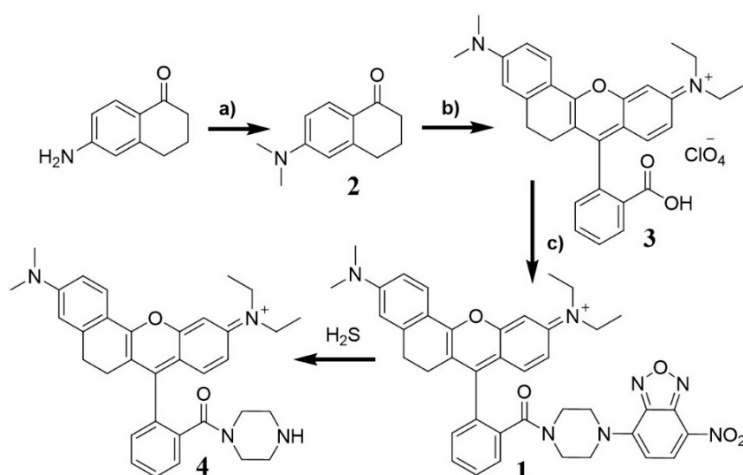
NIR dyes, including cyanine (Cy), are considered the classic NIR fluorescent dyes [60]. However, due to their flexible molecular structure, some of NIR fluorescent dyes accompanied some short comings for example, small Stokes shift, limited fluorescence quantum yield, low photo-stability lying, and high occupied molecular orbital (HOMO) energy levels [61,62]. Such photo-physical properties strongly affect the fluorescence signals due to the high background signal, which in turn result in low contrast for bioimaging [63–66]. In 2017, we developed a Cy-NBD probe (Scheme 1) which has the limitation of low quantum yield after H₂S activation [58]. On the other side, classical rhodamine dyes contributed much in the field of biomolecular detection and biomedical imaging because of its magnificent photophysical and chemical properties [30,67–71]. Due to limited π-conjugated system of xanthene core derivatives, such as rhodamine B, rhodamine 6G, and rhodamine 123 have their emission wavelengths in the visible region (<600 nm). Recently, significant advancements have been made in the improvement of rhodamines-based fluorescent dyes with extended the π-conjugated system possessing long emission wavelength, high fluorescence quantum yield, and outstanding photostability [70–75]. Herein, we report the development of an extended π-conjugated rhodamine-NBD based probe 1 for

the highly selective imaging of endogenous H₂S in a red shifted region [70,71]. The probe is high selectivity towards H₂S among other biothiols, with fluorescence emission in the red shifted region (>660 nm) and high fluorescence quantum yield (0.29) after H₂S activation. The probe is successfully used for bioimaging of endogenous H₂S in living cells.

2. Results and Discussion

2.1. Synthesis of 1

Probe 1 was constructed using a three-step route with a good yield (Scheme 2). By using the procedure described in the literature [76], 6-(dimethylamino)-3,4-dihydronaphthalen-1(2H)-one 2 was first synthesized from commercially available 6-amino-3,4-dihydronaphthalen-1(2H)-one, which was then transformed to 3. Finally, the probe 1 in 79% yield, was prepared by the coupling of compound 3 with NBD-piperazine. The facile and economic synthesis is important for the wide use of the probe. The structure of compound 1 was confirmed by ¹H NMR, ¹³C NMR, and high resolution mass spectrum (HRMS). The spectra (Figure S8) are included in the Supplemental Information.



Scheme 2. Synthetic route for probe 1 and its reaction with H₂S. Reagents and conditions: a) 6-aminotetralone, CH₃I, K₂CO₃, DMF, 0 °C, 24 h, 53%. b) 2-(4-(diethylamino)-2-hydroxybenzoyl)-benzoic acid, N-substituent ketone, H₂SO₄ 0–100 °C, 2 h, 80%. c) NBD-piperazine, HATU, DIPEA, DMF, 79%.

2.2. UV-Vis and Fluorescence Response of 1 towards H₂S

With the probe in hand, we first tested the solubility of 1 in buffer solution. The linearity of 1 verified its good solubility up to 20 μM (Figure S1). Further, we tested the optical properties of 1, and the absorbance and emission profiles are illustrated in Figure 1. As shown in Figure 1A, 1 displayed UV absorbance maxima at 620 nm and 500 nm, which are assigned to the rhodamine and NBD absorbance respectively. Since Na₂S is a well-known inorganic H₂S donor that is widely employed in the study of H₂S effects on physiology, we used it as a H₂S equivalent [77]. When reacted with H₂S, the increase in intensity of absorbance peaks appeared between 600 nm and 520 nm, which could be assigned to the yielding of 4 and NBD-SH. The reaction between 1 and 500 μM H₂S in PBS buffer (50 mM, pH 7.4) finished within 5 min. Furthermore, such thiolysis reaction was characterized by NMR with the formation of NBD-SH peaks (Figure S7) and HRMS with the production of peak at 535.3070 (calculated value for [4]⁺: 535.3068) (Figure S2).

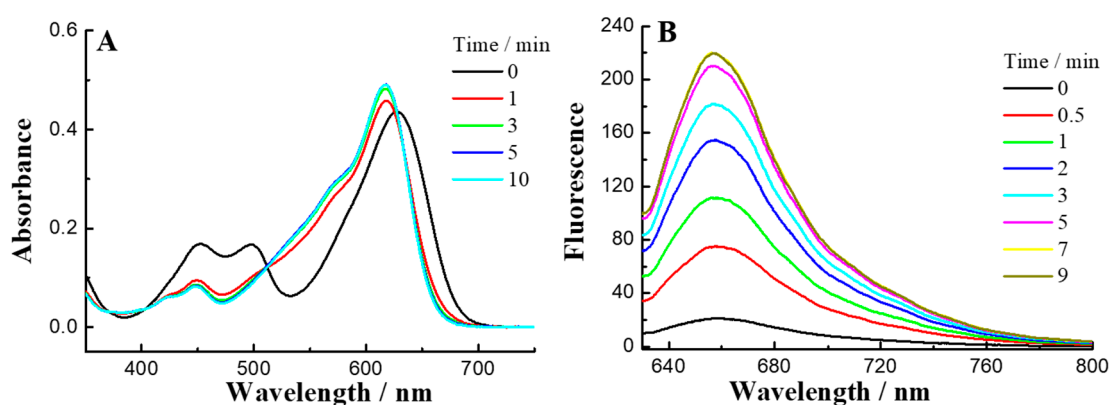


Figure 1. (A) Time-dependent absorbance spectra of **1** (5 μM) and H_2S (500 μM) in PBS (50 mM, pH 7.4, containing 10% DMSO). (B) Time-dependent fluorescence spectra (excitation = 620 nm) of **1** (2 μM) and H_2S (200 μM).

The probe **1** showed weak fluorescence (quantum yield ϕ , 0.021) upon excitation at 620 nm, indicating that fluorescence in **1** could be mainly quenched by the photoinduced electron transfer process (PET) effect from the NBD moiety [58]. When **1** reacted with H_2S , an excellent fluorescence change in a red shifted range with high brightness was observed (Figure 1B) with 10-fold turn-ons at 660 nm, and the quantum yield of the red shifted product was 0.29. The absorbance and emission data suggested the Stokes shift up to 40 nm in PBS. A large Stokes shift could reduce the risk of background fluorescence and thus avoid self-quenching and backscattering effect upon excitation. These preliminary studies suggest the extended π -conjugated system of rhodamines provides excellent red shifted fluorescence probes for detection in long range with high brightness.

2.3. Kinetics Studies

Reaction kinetics, as an important parameter, was investigated for the probe **1** with H_2S on account of its biological applicability under physiological conditions. To this end, the time-dependent fluorescence at 660 nm was recorded for data analysis (Figure 2A). The pseudo-first-order rate, k_{obs} , was found by fitting the data with a single exponential function. Plotting $\log[\text{H}_2\text{S}]$ versus $\log[k_{\text{obs}}]$ confirmed a first-order dependence in H_2S (Figure 2B). The reaction rate k_2 ($29.8 \text{ M}^{-1}\text{s}^{-1}$) was obtained by linear fitting of the k_{obs} versus H_2S concentration (Figure 2C). The H_2S -reaction rate of **1** is faster than our previous Rh-NBD-based probe [30], implying that such NBD-based probes can be employed for fast detection of H_2S . On the other hand, HPLC was further employed to identify the fast reaction of **1** with H_2S (Figure S4). Furthermore, fluorescent titration (Figure 3) was performed to determine the limit of detection (LOD) of **1** for H_2S as 0.27 μM by using the $3\sigma/k$ method [58].

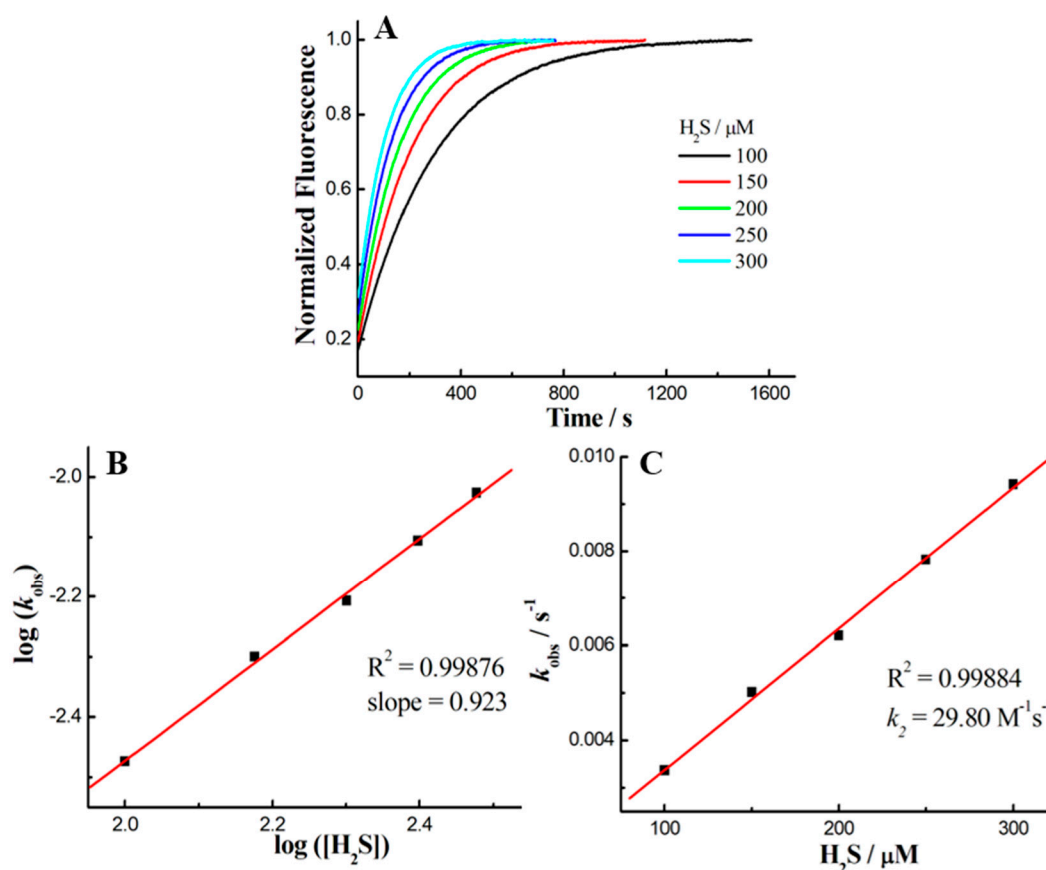


Figure 2. (A) The time-dependent fluorescence intensities at 660 nm for **1** (2 μM) in the presence of different concentrations of H₂S in PBS (50 mM, pH 7.4, containing 10% DMSO). (B) The linear relationship of log(k_{obs}) versus log([H₂S]). (C) The linear relationship of k_{obs} versus H₂S concentrations.

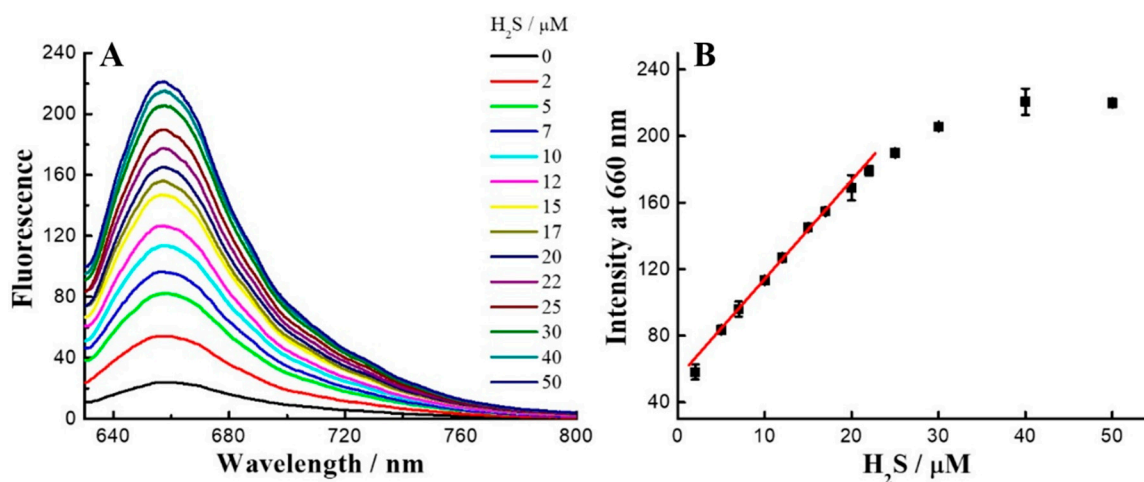


Figure 3. (A) The fluorescence changes of probe **1** (2 μM) responses to various concentrations of H₂S (0–50 μM) in PBS (50 mM, pH 7.4, containing 10% DMSO). (B) The linear relationship between concentrations of H₂S and emission at 660 nm. The detection limit was calculated to be 0.27 μM.

2.4. Selectivity and Co-Interference Studies

With above promising outcomes, we further investigated the selectivity and sensitivity of probe **1**. The fluorescent “off–on” response of **1** towards biothiols was measured. Probe **1** (2 μM) was treated with Cys, Hcy, and GSH individually (each 1 mM). As shown in Figure 4, the results showed that

fluorescence intensity enhancement for analytes was nearly negligible except H₂S, suggesting that **1** can selectively sense H₂S. In order to check the interference of biothiols with coexistent H₂S, we also tested **1** with these analytes in the presence of H₂S (Figure 4). These findings suggested that all analytes did not interfere the H₂S-specific thiolysis reaction. Furthermore, pH-dependent experiments were carried out to check whether **1** could sense at physiological pH (Figure S5). Obviously, the fluorescence enhancement occurred at pH 7.0–9.0, implying that **1** could work efficiently at physiological conditions.

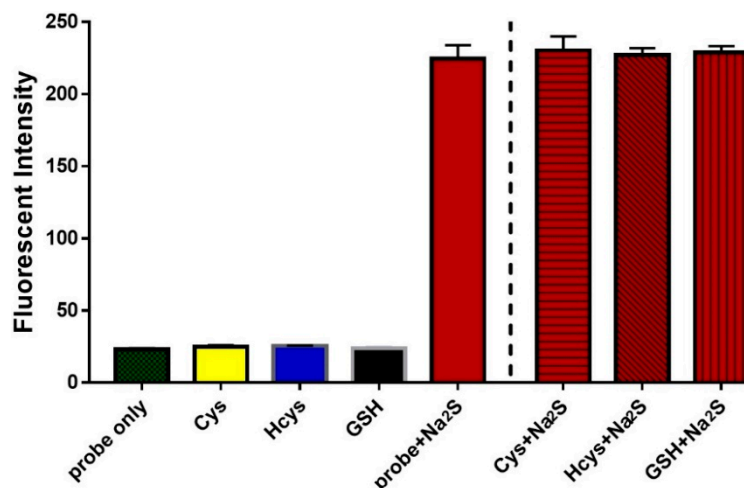


Figure 4. Fluorescence intensity at 660 nm of **1** (2 μ M) upon reacting with biothiols (1 mM) or H₂S (200 μ M) or biothiols with coexistent H₂S species in PBS buffer (pH 7.4) for 30 min.

2.5. Imaging of Probe **1** in Living Cells

Encouraged by the above results, we moved forward to study the biological applications of **1**. The cytotoxicity of the **1** was evaluated firstly by using the normal human umbilical vein endothelial cell (HUVEC) line via a standard MTT assay (Figure S6). After 24 h incubation with a varied concentration range of **1** from 5 μ M, over 85% of the cells still remained viable, implying the relatively good biocompatibility of **1**.

To examine the application potential of **1** for H₂S detection in living cells, HeLa cells were chosen as the model biological system. Briefly, the cells were incubated with **1** alone or co-incubated with **1** and Na₂S/D-Cys for 30 min. Then, all cells were examined via the confocal microscopy. Cells with probe **1** treatment displayed faint fluorescence (Figure 5E), while cells displayed remarkable red fluorescence in the presence of **1** and Na₂S (Figure 5F). These results demonstrated that **1** could be used for selective imaging of exogenous H₂S. For detection of endogenous production of H₂S, cells were co-incubated with D-Cys and **1**, as D-Cys can induce H₂S biosynthesis via the 3-MST pathway [4]. Strong fluorescence was observed in cells (Figure 5G), which revealed that the endogenous production of H₂S from D-Cys could be detected by **1**. To further confirm the detection of endogenous production of H₂S from D-Cys by **1**, an inhibitor (aminooxyacetic acid, AOAA) was introduced to block the pathway for H₂S production from D-Cys [4]. No obvious fluorescence was detected in the AOAA-treated cells (Figure 5H). These preliminary studies suggested that probe **1** could be used for visualization of H₂S in cells efficiently and selectively.

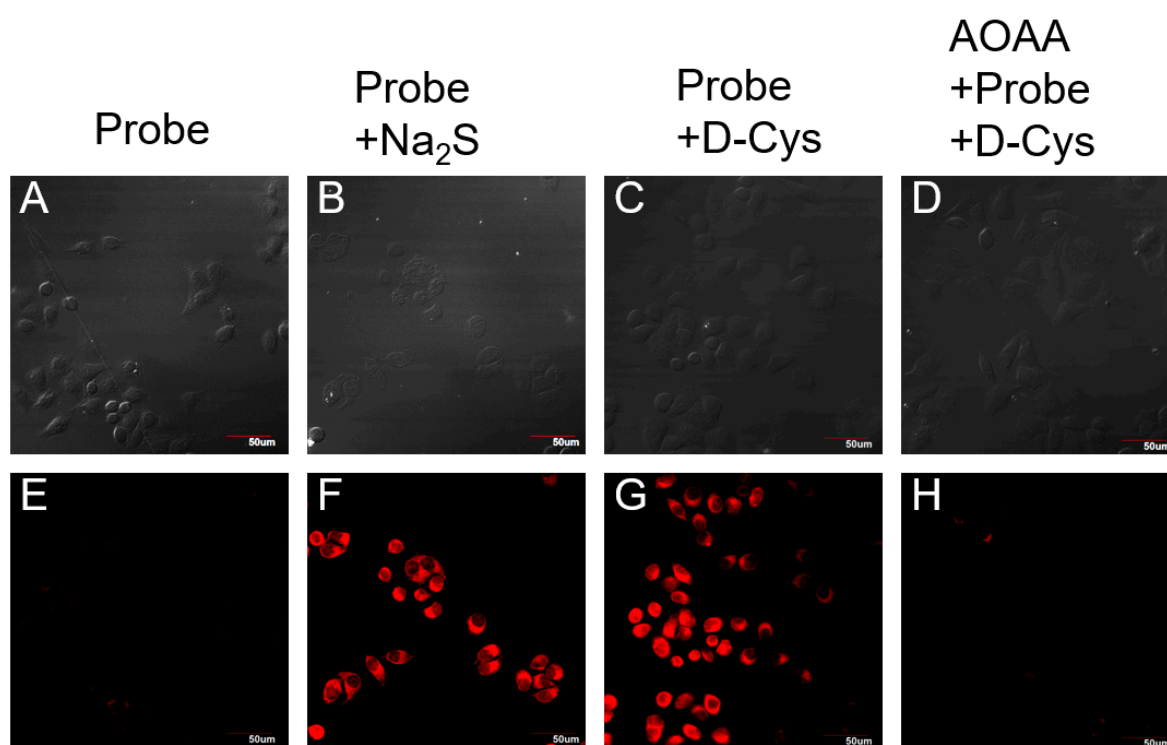


Figure 5. Fluorescence images of probe **1** for H₂S detection in living cells. Bright-field and fluorescence images of cells upon incubation with **1** (5 μM) for 30 min (**A,E**); with **1** and Na₂S (100 μM) (**B,F**); with **1** and D-Cys (100 μM) (**C,G**); with inhibitor (AOAA), **1** and D-Cys (100 μM) (**D,H**). Scale bars: 50 μm.

The probe **1** contains a positive charge, which might be mitochondria-targeting [33]. To this end, a fluorescent co-localization assay with Mito-Tracker Green FM (a well-known mitochondria specific dye) and probe **1** with D-Cys was carried out. As shown in Figure 6, the green fluorescence signal produced by Mito-Tracker Green FM and the red fluorescence signal from probe **1** merged well in the cells (Figure 6C). The Pearson's coefficient is 0.946. These data implied that the probe **1** is a promising tool for imaging of mitochondria H₂S.

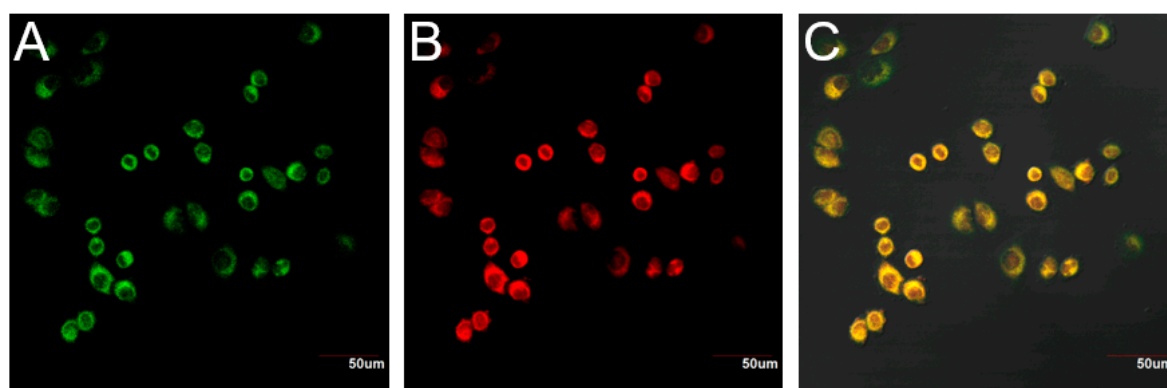


Figure 6. Confocal microscopy images of mitochondrion by **1** in living cells. Cells were co-stained with **1** (5 μM), D-Cys (100 μM) and commercial MitoTracker[®] Green FM (2.5 μM). (**A**) The cell image displayed by green channel (500–530 nm, excitation at 488 nm). (**B**) The cell image displayed by red channel (620–660 nm, excitation at 594 nm). (**C**) Merged graph of fluorescence images of **1** and MitoTracker[®] Green FM. Scale bars: 50 μm.

3. Experimental

3.1. Materials and Methods

All chemicals and solvents used for the synthesis were purchased from commercial suppliers and applied directly in the experiments without further purification. The progress of the reaction was monitored by TLC on pre-coated silica plates (60F-254, 250 μm) in thickness (Merck, Darmstadt, Germany), and spots were visualized by basic KMnO_4 , UV light or iodine. Merck silica gel 60 (100–200 mesh) was used for general column chromatography purification. ^1H NMR and ^{13}C NMR spectra were recorded on a Bruker 400 spectrometer (Karlsruhe, Germany). Chemical shifts are reported in parts per million with respect to the internal standard tetramethylsilane ($\text{Si}(\text{CH}_3)_4 = 0.00$ ppm) or residual solvent peaks ($\text{CD}_2\text{Cl}_2 = 5.32$ ppm; $\text{CDCl}_3 = 7.26$ ppm; $\text{DMSO-d}_6 = 2.5$ ppm). ^1H NMR coupling constants (J) are reported in hertz (Hz), and multiplicity is indicated as the following: s (singlet), d (doublet), t (triplet), dd (doublet of doublets), m (multiple). High-resolution mass spectra (HRMS) were obtained on an Agilent 6540 UHD Accurate-Mass Q-TOF LC/MS or Varian 7.0 T FTICR-MS. The UV-visible spectra were recorded on a UV-3600 UV-VIS-NIR spectrophotometer (Shimadzu, Japan). The fluorescence study was carried out using an F-280 spectrophotometer (Tianjin Gangdong Sci & Tech., Development. Co., Ltd. Tianjin, China).

3.2. Synthesis of 6-(dimethylamino)-3,4-Dihydronaphthalen-1(2H)-One

To a mixture of 6-aminotetralone (0.50 g, 3.1 mmol), CH_3I (0.06 g, 4.6 mmol) and K_2CO_3 (1.3 g, 9.3 mmol) in DMF (5 mL) was stirred for 24 h at 40–45 $^\circ\text{C}$. After completion of reaction, the mixture was cooled to room temperature, water (10 mL) was added and the solution was extracted with EtOAc (3 \times 50 mL). The organic layers were combined, dried with anhydrous MgSO_4 and the solvent was removed under reduced pressure. The residue was purified by silica gel column chromatography using PE (petroleum ether): EtOAc = 6:1 as the eluent to obtain pure compound (Yield: 53.0%, 0.31 g). ^1H NMR (400 MHz, CDCl_3) δ 7.95 (dd, J = 8.8, 1.6 Hz, 1H), 6.62 (d, J = 8.8 Hz, 1H), 6.43 (s, 1H), 3.06 (s, 6H), 2.88 (t, J = 5.2 Hz, 2H), 2.59–2.55 (m, 2H), 2.10–2.05 (m, 2H). ^{13}C NMR (101 MHz, CDCl_3) δ 196.9, 153.5, 146.6, 129.4, 121.9, 110.3, 109.6, 40.2, 38.9, 30.7, 23.7. HRMS $[\text{C}_{12}\text{H}_{16}\text{NO}]^+$: Calcd. for $[\text{M}+\text{H}]^+$ 190.1232; found: $[\text{M}+\text{H}]^+$ 190.1228.

3.3. Synthesis of Intermediate 3

2-(4-diethylamino-2-hydroxybenzoyl)-benzoic acid (0.151 g, 0.48 mmol) and 6-(dimethylamino)-3,4-dihydronaphthalen-1(2H)-one (0.091 g, 0.48 mmol) were added to concentrated H_2SO_4 (10 mL) at 0 $^\circ\text{C}$. The mixture was stirred at 100 $^\circ\text{C}$ for 2 h. After completion of reaction the mixture was allowed to cool at room temperature and was poured onto ice (10 g). HClO_4 (1 mL) was gently added to the solution and the resulting precipitate was filtered off and washed with cold water. After drying, the residue was purified by silica gel column chromatography using CH_2Cl_2 : methanol = 20:1 as the eluent to obtain pure compound as a purple-green solid (Yield: 80.0%, 0.17 g). ^1H NMR (400 MHz, DMSO-d_6) δ 13.22 (s, 1H), 8.19 (dd, J = 7.2, 2.4 Hz, 2H), 7.86 (t, J = 7.2 Hz, 1H), 7.75 (t, J = 7.6 Hz, 1H), 7.41 (d, J = 7.2 Hz, 1H), 7.24 (d, J = 1.6 Hz, 1H), 7.09 (d, J = 9.6 Hz, 1H), 6.93 (dd, J = 9.2, 2.0 Hz, 1H), 6.87 (d, J = 9.2 Hz, 1H), 6.75 (s, 1H), 3.58 (q, J = 6.4 Hz, 4H), 3.18 (s, 6H), 2.93–2.80 (m, 2H), 2.49–2.35 (m, 2H), 1.19 (t, J = 6.9 Hz, 6H). ^{13}C NMR (101 MHz, DMSO-d_6) δ 166.5, 163.4, 156.1, 155.0, 153.1, 145.1, 134.4, 133.0, 130.9, 130.0, 129.2, 129.1, 128.6, 118.4, 115.2, 114.3, 113.0, 112.0, 110.7, 96.0, 44.8, 40.0, 26.9, 23.6, 12.4. HRMS $[\text{C}_{30}\text{H}_{31}\text{N}_2\text{O}_3]^+$: Calcd. for $[\text{M}]^+$ 467.2329; found: $[\text{M}]^+$ 467.2331.

3.4. Synthesis of Probe 1

Dissolved compound 2 (0.121 g, 0.2 mmol) in 5 mL DMF, followed by the addition of HATU (0.122 g, 0.32 mmol) and DIPEA (102 μL , 0.75 mmol). Stirred the solution for 5 min, NBD-piperazine (0.064 g, 0.2 mmol) was added to the solution and continue the stirring for 12 h at room temperature. After completion of reaction DMF was removed in vacuo. The residue was purified by silica gel

column chromatography to give dark-red solid **1** (0.12 g, 79%). ^1H NMR (400 MHz, DMSO- d_6) δ 8.50 (d, $J = 8.8$ Hz, 1H), 8.16 (d, $J = 8.8$ Hz, 1H), 7.74 (bs, 3H), 7.48 (bs, 1H), 7.20 (bs, 1H), 7.07 (bs, 2H), 6.91 (d, $J = 8.0$ Hz, 1H), 6.72 (s, 1H), 6.54 (d, $J = 9.2$ Hz, 1H), 4.22–4.14 (m, 2H), 4.03–3.83 (m, 2H), 3.82–3.46 (m, 8H), 3.19 (s, 6H), 2.98–2.78 (m, 2H), 2.62–2.45 (m, 2H), 1.16 (s, 6H). ^{13}C NMR (101 MHz, DMSO- d_6) δ 167.0, 163.8, 156.0, 155.2, 153.0, 145.5, 145.3, 144.7, 136.2, 134.2, 131.9, 130.2, 129.5, 129.3, 129.3, 129.2, 127.6, 121.5, 119.6, 114.9, 114.3, 113.0, 112.1, 110.7, 103.4, 96.1, 49.0, 48.1, 45.6, 44.8, 40.8, 27.0, 23.9, 12.4. HRMS [$\text{C}_{40}\text{H}_{40}\text{N}_7\text{O}_5$] $^+$: Calcd. for [M] $^+$ 698.3085; found: [M] $^+$ 698.3090.

3.5. Procedure for Spectroscopic Studies

All spectroscopic measurements were performed in phosphate-buffered saline buffer (PBS, 50 mM, pH 7.4, containing 10% DMSO) at room temperature. Compounds were dissolved into DMSO to prepare the stock solutions with a concentration of 5 mM. 1–500 mM Stock solutions of Na_2S in degassed (by bubbling N_2 for 30 min) PBS buffer were used as H_2S source. Probes were diluted in PBS buffer (50 mM, pH 7.4, containing 10% DMSO) to afford the final concentration of 2–5 μM . For the selectivity experiment, different biologically relevant molecules (100 mM) were prepared as stock solutions in degassed PBS buffer. Appropriate amount of biologically relevant species was added to separate portions of the probe solution and mixed thoroughly. All measurements were performed in a 3 mL corvette with 2 mL solution. The reaction mixture was shaken uniformly before emission spectra were measured.

3.6. Cell Culture and Cytotoxicity Assay

The HUVEC and HeLa cell lines were purchased from the Cell Bank of the Chinese Academy of Sciences (Shanghai, China). And the cells were cultured in RPMI 1640 medium with 10% fetal bovine serum and 1% penicillin/streptomycin under standard cell culture conditions at 37 °C in a humidified CO_2 incubator. Before the cytotoxicity assay, the HUVEC cells were transferred to the 96-well plate and cultured for one night. After that, the culture medium was replaced with a fresh one and the HUVEC cells were pre-incubated with probe **1** with a concentration range of 5–25 μM for 24 h. The cell viability was then measured by the standard MTT assay.

3.7. Cell Imaging

Glass bottom dishes were added into a 24-well plate for cell imaging before cells were seeded. Then, the HeLa cells were transferred to the 24-well plate and cultured for one night before the experiments. After that, the culture medium was replaced with the fresh one and the cells were treated with the desired reagents. After incubation, the HeLa cells were quickly washed with PBS three times, and then fixed with 4% paraformaldehyde solution for 10 min. Finally, the HeLa cells were washed with PBS and imaged using a confocal microscope (Olympus FV1000) with a 40 \times objective lens. Emission was collected at the green channel (500–530 nm, excitation at 488 nm) and the red channel (620–660 nm, excitation at 594 nm).

4. Conclusions

In summary, we have developed a new, extended π -conjugation rhodamine-NBD a red shifted fluorescence probe **1** capable of detection H_2S in live cells. The probe shows a relatively large Stokes shift (40 nm), fast response ($k = 29.8 \text{ M}^{-1}\text{s}^{-1}$), and good quantum yield ($\phi = 0.29$) after H_2S activation. Moreover, **1** was water-soluble, cell-membrane-permeable, and had high selectivity and sensitivity for H_2S . We believe that this red shifted range probe **1** could be a useful tool for studies of H_2S biology in the future.

Supplementary Materials: Supplementary data associated with this article can be found in the online.

Author Contributions: Formal preparation and writing—original draft, (I.I.); writing—review and editing (L.Y., L.S. & Z.C.); Bioimaging (I.I., X.J. & L.S.); Supervision and funding acquisition (L.Y. & Z.X.). All authors have read and agreed to the published version of the manuscript.

Funding: This research was supported by the NFSC (21702111).

Acknowledgments: We thank the prospective project supported by the National Natural Science Foundation of China (21702111).

Conflicts of Interest: The authors declare no conflict of interest.

References

1. Wang, R. Physiological Implications of Hydrogen Sulfide: A Whiff Exploration That Blossomed. *Physiol. Rev.* **2012**, *92*, 791–896. [[CrossRef](#)] [[PubMed](#)]
2. Szabo, C. Gasotransmitters in cancer: From pathophysiology to experimental therapy. *Nat. Rev. Drug Discov.* **2016**, *15*, 185–203. [[CrossRef](#)] [[PubMed](#)]
3. Li, L.; Rose, P.; Moore, P.K. Hydrogen sulfide and cell signaling. *Annu. Rev. Pharmacol. Toxicol.* **2011**, *51*, 169–187. [[CrossRef](#)] [[PubMed](#)]
4. Shibuya, N.; Koike, S.; Tanaka, M.; Ishigami-Yuasa, M.; Kimura, Y.; Ogasawara, Y.; Fukui, K.; Nagahara, N.; Kimura, H. A novel pathway for the production of hydrogen sulfide from D-cysteine in mammalian cells. *Nat. Commun.* **2013**, *4*, 1366. [[CrossRef](#)] [[PubMed](#)]
5. Wu, L.; Yang, W.; Jia, X.; Yang, G.; Duridanova, D.; Cao, K.; Wang, R. Pancreatic islet overproduction of H₂S and suppressed insulin release in Zucker diabetic rats. *Lab. Invest.* **2009**, *89*, 59–67. [[CrossRef](#)]
6. Eto, K.; Asada, T.; Arima, K.; Makifuchi, T.; Kimura, H. Brain hydrogen sulfide is severely decreased in Alzheimer’s disease. *Biochem. Biophys. Res. Commun.* **2002**, *293*, 1485–1488. [[CrossRef](#)]
7. Fiorucci, S.; Antonelli, E.; Mencarelli, A.; Orlandi, S.; Renga, B.; Rizzo, G.; Distrutti, E.; Shah, V.; Morelli, A. The third gas: H₂S regulates perfusion pressure in both the isolated and perfused normal rat liver and in cirrhosis. *Hepatology* **2005**, *42*, 539–548. [[CrossRef](#)]
8. Wang, X.; Sun, J.; Zhang, W.; Ma, X.; Lv, J.; Tang, B. A near-infrared ratiometric fluorescent probe for rapid and highly sensitive imaging of endogenous hydrogen sulfide in living cells. *Chem. Sci.* **2013**, *4*, 2551–2556. [[CrossRef](#)]
9. Zhang, H.; Xie, Y.; Wang, P.; Chen, G.; Liu, R.; Lam, Y.W.; Hu, Y.; Zhu, Q.; Sun, H. An iminocoumarin benzothiazole-based fluorescent probe for imaging hydrogen sulfide in living cells. *Talanta* **2015**, *135*, 149–154. [[CrossRef](#)]
10. Coletta, C.; Modis, K.; Szczesny, B.; Brunyanszki, A.; Olah, G.; Rios, E.C.; Yanagi, K.; Ahmad, A.; Papapetropoulos, A.; Szabo, C. Regulation of Vascular Tone, Angiogenesis and Cellular Bioenergetics by the 3-Mercaptopyruvate Sulfurtransferase/H₂S Pathway: Functional Impairment by Hyperglycemia and Restoration by DL- α -Lipoic Acid. *Mol. Med.* **2015**, *21*, 1–14. [[CrossRef](#)]
11. Wu, D.; Si, W.; Wang, M.; Lv, S.; Ji, A.; Li, Y. Hydrogen sulfide in cancer: Friend or foe? *Nitric Oxide* **2015**, *50*, 38–45. [[CrossRef](#)] [[PubMed](#)]
12. Hancock, J.T.; Whiteman, M. Hydrogen sulfide and cell signaling: Team player or referee? *Plant Physiol. Biochem.* **2014**, *78*, 37–42. [[CrossRef](#)] [[PubMed](#)]
13. Calderwood, A.; Kopriva, S. Hydrogen sulfide in plants: From dissipation of excess sulfur to signaling molecule. *Nitric Oxide.* **2014**, *41*, 72–78. [[CrossRef](#)] [[PubMed](#)]
14. Romero, L.C.; Garcia, I.; Gotor, C. L-Cysteine Desulfhydrase 1 modulates the generation of the signaling molecule sulfide in plant cytosol. *Plant Signal. Behav.* **2013**, *8*, e24007. [[CrossRef](#)]
15. Shukla, P.; Khodade, V.S.; SharathChandra, M.; Chauhan, P.; Mishra, S.; Siddaramappa, S.; Pradeep, B.E.; Singh, A.; Chakrapani, H. “On demand” redox buffering by H₂S contributes to antibiotic resistance revealed by a bacteria-specific H₂S donor. *Chem. Sci.* **2017**, *8*, 4967–4972. [[CrossRef](#)]
16. Lin, V.S.; Chen, W.; Xian, M.; Chang, C.J. Chemical probes for molecular imaging and detection of hydrogen sulfide and reactive sulfur species in biological systems. *Chem. Soc. Rev.* **2015**, *44*, 4596–4618. [[CrossRef](#)]
17. Yu, F.; Han, X.; Chen, L. Fluorescent probes for hydrogen sulfide detection and bioimaging. *Chem. Commun.* **2014**, *50*, 12234–12249. [[CrossRef](#)]
18. Hartle, M.D.; Pluth, M.D. A practical guide to working with H₂S at the interface of chemistry and biology. *Chem. Soc. Rev.* **2016**, *45*, 6108–6117. [[CrossRef](#)]

19. Zhao, Y.; Biggs, T.D.; Xian, M. Hydrogen sulfide (H₂S) releasing agents: Chemistry and biological applications. *Chem. Commun.* **2014**, *50*, 11788–11805. [[CrossRef](#)]
20. Cerda, M.M.; Newton, T.D.; Zhao, Y.; Collins, B.K.; Hendon, C.H.; Pluth, M.D. Dithioesters: Simple, tunable, cysteine-selective H₂S donors. *Chem. Sci.* **2019**, *10*, 1773–1779. [[CrossRef](#)]
21. Levinn, C.M.; Cerda, M.M.; Pluth, M.D. Development and Application of Carbonyl Sulfide-Based Donors for H₂S Delivery. *Acc. Chem. Res.* **2019**, *52*, 2723–2731. [[CrossRef](#)] [[PubMed](#)]
22. Ke, B.; Wu, W.; Liu, W.; Liang, H.; Gong, D.; Hu, X.; Li, M. Bioluminescence Probe for Detecting Hydrogen Sulfide in Vivo. *Anal. Chem.* **2016**, *88*, 592–595. [[CrossRef](#)] [[PubMed](#)]
23. Sasakura, K.; Hanaoka, K.; Shibuya, N.; Mikami, Y.; Kimura, Y.; Komatsu, T.; Ueno, T.; Terai, T.; Kimura, H.; Nagano, T. Development of a highly selective fluorescence probe for hydrogen sulfide. *J. Am. Chem. Soc.* **2011**, *133*, 18003–18005. [[CrossRef](#)] [[PubMed](#)]
24. Wang, C.; Cheng, X.; Tan, J.; Ding, Z.; Wang, W.; Yuan, D.; Li, G.; Zhang, H.; Zhang, X. Reductive cleavage of C=C bonds as a new strategy for turn-on dual fluorescence in effective sensing of H₂S. *Chem. Sci.* **2018**, *9*, 8369–8374. [[CrossRef](#)]
25. Liu, J.; Guo, X.; Hu, R.; Liu, X.; Wang, S.; Li, S.; Li, Y.; Yang, G. Molecular Engineering of Aqueous Soluble Triarylboron-Compound-Based Two-Photon Fluorescent Probe for Mitochondria H₂S with Analyte-Induced Finite Aggregation and Excellent Membrane Permeability. *Anal. Chem.* **2016**, *88*, 1052–1057. [[CrossRef](#)]
26. Mao, Z.; Ye, M.; Hu, W.; Ye, X.; Wang, Y.; Zhang, H.; Li, C.; Liu, Z. Design of a ratiometric two-photon probe for imaging of hypochlorous acid (HClO) in wounded tissues. *Chem. Sci.* **2018**, *9*, 6035–6040. [[CrossRef](#)]
27. Zhao, Y.; Cerda, M.M.; Pluth, M.D. Fluorogenic hydrogen sulfide (H₂S) donors based on sulfenyl thiocarbonates enable H₂S tracking and quantification. *Chem. Sci.* **2019**, *10*, 1873–1878. [[CrossRef](#)]
28. Cao, X.; Lin, W.; Zheng, K.; He, L. A near-infrared fluorescent turn-on probe for fluorescence imaging of hydrogen sulfide in living cells based on thiolysis of dinitrophenyl ether. *Chem. Commun.* **2012**, *48*, 10529–10531. [[CrossRef](#)]
29. Shi, B.; Gu, X.; Fei, Q.; Zhao, C. Photoacoustic probes for real-time tracking of endogenous H₂S in living mice. *Chem. Sci.* **2017**, *8*, 2150–2155. [[CrossRef](#)]
30. Ismail, I.; Wang, D.; Wang, D.; Niu, C.; Huang, H.; Yi, L.; Xi, Z. A mitochondria-targeted red-emitting probe for imaging hydrogen sulfide in living cells and zebrafish. *Org. Biomol. Chem.* **2019**, *17*, 3389–3395. [[CrossRef](#)]
31. Ismail, I.; Wang, D.; Wang, Z.; Wang, D.; Zhang, C.; Yi, L.; Xi, Z. A julolidine-fused coumarin-NBD dyad for highly selective and sensitive detection of H₂S in biological samples. *Dyes Pigment.* **2019**, *163*, 700–706. [[CrossRef](#)]
32. Pak, Y.L.; Li, J.; Ko, K.C.; Kim, G.; Lee, J.Y.; Yoon, J. Mitochondria-Targeted Reaction-Based Fluorescent Probe for Hydrogen Sulfide. *Anal. Chem.* **2016**, *88*, 5476–5481. [[CrossRef](#)] [[PubMed](#)]
33. Yi, L.; Xi, Z. Thiolysis of NBD-based dyes for colorimetric and fluorescence detection of H₂S and biothiols: Design and biological applications. *Org. Biomol. Chem.* **2017**, *15*, 3828–3839. [[CrossRef](#)] [[PubMed](#)]
34. Karakus, E.; Ucuncu, M.; Emrullahoglu, M. Electrophilic Cyanate As a Recognition Motif for Reactive Sulfur Species: Selective Fluorescence Detection of H₂S. *Anal. Chem.* **2016**, *88*, 1039–1043. [[CrossRef](#)]
35. He, L.; Yang, X.; Xu, K.; Kong, X.; Lin, W. A multi-signal fluorescent probe for simultaneously distinguishing and sequentially sensing cysteine/homocysteine, glutathione, and hydrogen sulfide in living cells. *Chem. Sci.* **2017**, *8*, 6257–6265. [[CrossRef](#)]
36. Zhang, C.; Zhang, Q.Z.; Zhang, K.; Li, L.Y.; Pluth, M.D.; Yi, L.; Xi, Z. Dual-biomarker-triggered fluorescence probes for differentiating cancer cells and revealing synergistic antioxidant effects under oxidative stress. *Chem. Sci.* **2019**, *10*, 1945–1952. [[CrossRef](#)]
37. Manley, M. Near-infrared spectroscopy and hyperspectral imaging: Non-destructive analysis of biological materials. *Chem. Soc. Rev.* **2014**, *43*, 8200–8214. [[CrossRef](#)]
38. Slooter, M.D.; Bierau, K.; Chan, A.B.; Lowik, C.W. Near infrared fluorescence imaging for early detection, monitoring and improved intervention of diseases involving the joint. *Connect. Tissue Res.* **2015**, *56*, 153–160. [[CrossRef](#)]
39. Yuan, L.; Lin, W.; Zheng, K.; He, L.; Huang, W. Far-red to near infrared analyte-responsive fluorescent probes based on organic fluorophore platforms for fluorescence imaging. *Chem. Soc. Rev.* **2013**, *42*, 622–661. [[CrossRef](#)]
40. Guo, Z.; Park, S.; Yoon, J.; Shin, I. Recent progress in the development of near-infrared fluorescent probes for bioimaging applications. *Chem. Soc. Rev.* **2014**, *43*, 16–29. [[CrossRef](#)]

41. Staudinger, C.; Borisov, S.M. Long-wavelength analyte-sensitive luminescent probes and optical (bio)sensors. *Methods Appl. Fluoresc.* **2015**, *3*, 042005. [[CrossRef](#)] [[PubMed](#)]
42. Owens, E.A.; Henary, M.; El Fakhri, G.; Choi, H.S. Tissue-Specific Near-Infrared Fluorescence Imaging. *Acc. Chem. Res.* **2016**, *49*, 1731–1740. [[CrossRef](#)] [[PubMed](#)]
43. Fu, M.; Xiao, Y.; Qian, X.; Zhao, D.; Xu, Y. A design concept of long-wavelength fluorescent analogs of rhodamine dyes: Replacement of oxygen with silicon atom. *Chem. Commun.* **2008**, *15*, 1780–1782. [[CrossRef](#)] [[PubMed](#)]
44. Koide, Y.; Urano, Y.; Hanaoka, K.; Terai, T.; Nagano, T. Evolution of group 14 rhodamines as platforms for near-infrared fluorescence probes utilizing photoinduced electron transfer. *ACS Chem. Biol.* **2011**, *6*, 600–608. [[CrossRef](#)]
45. Miao, X.; Hu, W.; He, T.; Tao, H.; Wang, Q.; Chen, R.; Jin, L.; Zhao, H.; Lu, X.; Fan, Q.; et al. Deciphering the intersystem crossing in near-infrared BODIPY photosensitizers for highly efficient photodynamic therapy. *Chem. Sci.* **2019**, *10*, 3096–3102. [[CrossRef](#)]
46. Koide, Y.; Urano, Y.; Hanaoka, K.; Piao, W.; Kusakabe, M.; Saito, N.; Terai, T.; Okabe, T.; Nagano, T. Development of NIR fluorescent dyes based on Si-rhodamine for in vivo imaging. *J. Am. Chem. Soc.* **2012**, *134*, 5029–5031. [[CrossRef](#)]
47. Xu, W.; Lee, M.M.S.; Zhang, Z.; Sung, H.H.Y.; Williams, I.D.; Kwok, R.T.K.; Lam, J.W.Y.; Wang, D.; Tang, B.Z. Facile synthesis of AIEgens with wide color tunability for cellular imaging and therapy. *Chem. Sci.* **2019**, *10*, 3494–3501. [[CrossRef](#)]
48. Yuan, L.; Lin, W.; Yang, Y.; Chen, H. A unique class of near-infrared functional fluorescent dyes with carboxylic-acid-modulated fluorescence ON/OFF switching: Rational design, synthesis, optical properties, theoretical calculations, and applications for fluorescence imaging in living animals. *J. Am. Chem. Soc.* **2012**, *134*, 1200–1211. [[CrossRef](#)]
49. Ruan, C.; Liu, C.; Hu, H.; Guo, X.L.; Jiang, B.P.; Liang, H.; Shen, X.C. NIR-II light-modulated thermosensitive hydrogel for light-triggered cisplatin release and repeatable chemo-photothermal therapy. *Chem. Sci.* **2019**, *10*, 4699–4706. [[CrossRef](#)]
50. Yuan, L.; Lin, W.; Zhao, S.; Gao, W.; Chen, B.; He, L.; Zhu, S. A unique approach to development of near-infrared fluorescent sensors for in vivo imaging. *J. Am. Chem. Soc.* **2012**, *134*, 13510–13523. [[CrossRef](#)]
51. Chevalier, A.; Renard, P.Y.; Romieu, A. Straightforward access to water-soluble unsymmetrical sulfoxanthene dyes: Application to the preparation of far-red fluorescent dyes with large Stokes' shifts. *Chemistry* **2014**, *20*, 8330–8337. [[CrossRef](#)]
52. Chen, Y.; Zhu, C.; Yang, Z.; Chen, J.; He, Y.; Jiao, Y.; He, W.; Qiu, L.; Cen, J.; Guo, Z. A ratiometric fluorescent probe for rapid detection of hydrogen sulfide in mitochondria. *Angew. Chem. Int. Ed.* **2013**, *52*, 1688–1691. [[CrossRef](#)] [[PubMed](#)]
53. He, X.; Li, L.; Fang, Y.; Shi, W.; Li, X.; Ma, H. In vivo imaging of leucine aminopeptidase activity in drug-induced liver injury and liver cancer via a near-infrared fluorescent probe. *Chem. Sci.* **2017**, *8*, 3479–3483. [[CrossRef](#)] [[PubMed](#)]
54. Li, P.; Wang, J.; Wang, X.; Ding, Q.; Bai, X.; Zhang, Y.; Su, D.; Zhang, W.; Zhang, W.; Tang, B. In situ visualization of ozone in the brains of mice with depression phenotypes by using a new near-infrared fluorescence probe. *Chem. Sci.* **2019**, *10*, 2805–2810. [[CrossRef](#)]
55. Sun, W.; Fan, J.; Hu, C.; Cao, J.; Zhang, H.; Xiong, X.; Wang, J.; Cui, S.; Sun, S.; Peng, X. A two-photon fluorescent probe with near-infrared emission for hydrogen sulfide imaging in biosystems. *Chem. Commun.* **2013**, *49*, 3890–3892. [[CrossRef](#)] [[PubMed](#)]
56. Wang, R.; Chen, J.; Gao, J.; Chen, J.A.; Xu, G.; Zhu, T.; Gu, X.; Guo, Z.; Zhu, W.H.; Zhao, C. A molecular design strategy toward enzyme-activated probes with near-infrared I and II fluorescence for targeted cancer imaging. *Chem. Sci.* **2019**, *10*, 7222–7227. [[CrossRef](#)] [[PubMed](#)]
57. Zheng, Y.; Zhao, M.; Qiao, Q.; Liu, H.; Lang, H.; Xu, Z. A near-infrared fluorescent probe for hydrogen sulfide in living cells. *Dyes Pigments* **2013**, *98*, 367–371. [[CrossRef](#)]
58. Zhang, K.; Zhang, J.; Xi, Z.; Li, L.Y.; Gu, X.; Zhang, Q.Z.; Yi, L. A new H₂S-specific near-infrared fluorescence-enhanced probe that can visualize the H₂S level in colorectal cancer cells in mice. *Chem. Sci.* **2017**, *8*, 2776–2781. [[CrossRef](#)]
59. Xie, Y.; Huang, H.; Ismail, I.; Sun, H.; Yi, L.; Xi, Z. A fluorogenic H₂S-triggered prodrug based on thiolysis of the NBD amine. *Bioorg. Med. Chem. Lett.* **2019**, *29*, 126627. [[CrossRef](#)]

60. Mishra, A.; Behera, R.K.; Behera, P.K.; Mishra, B.K.; Behera, G.B. Cyanines during the 1990s: A Review. *Chem. Rev.* **2000**, *100*, 1973–2012. [[CrossRef](#)]
61. Kiyose, K.; Aizawa, S.; Sasaki, E.; Kojima, H.; Hanaoka, K.; Terai, T.; Urano, Y.; Nagano, T. Molecular design strategies for near-infrared ratiometric fluorescent probes based on the unique spectral properties of aminocyanines. *Chemistry* **2009**, *15*, 9191–9200. [[CrossRef](#)] [[PubMed](#)]
62. Egawa, T.; Hanaoka, K.; Koide, Y.; Ujita, S.; Takahashi, N.; Ikegaya, Y.; Matsuki, N.; Terai, T.; Ueno, T.; Komatsu, T.; et al. Development of a far-red to near-infrared fluorescence probe for calcium ion and its application to multicolor neuronal imaging. *J. Am. Chem. Soc.* **2011**, *133*, 14157–14159. [[CrossRef](#)] [[PubMed](#)]
63. Ozmen, B.; Akkaya, E.U. Infrared fluorescence sensing of submicromolar calcium: Pushing the limits of photoinduced electron transfer. *Tetrahedron Lett.* **2000**, *41*, 9185–9188. [[CrossRef](#)]
64. Sasaki, E.; Kojima, H.; Nishimatsu, H.; Urano, Y.; Kikuchi, K.; Hirata, Y.; Nagano, T. Highly sensitive near-infrared fluorescent probes for nitric oxide and their application to isolated organs. *J. Am. Chem. Soc.* **2005**, *127*, 3684–3685. [[CrossRef](#)]
65. Tang, B.; Yu, F.; Li, P.; Tong, L.; Duan, X.; Xie, T.; Wang, X. A near-infrared neutral pH fluorescent probe for monitoring minor pH changes: Imaging in living HepG2 and HL-7702 cells. *J. Am. Chem. Soc.* **2009**, *131*, 3016–3023. [[CrossRef](#)]
66. Yu, F.; Li, P.; Li, G.; Zhao, G.; Chu, T.; Han, K. A near-IR reversible fluorescent probe modulated by selenium for monitoring peroxynitrite and imaging in living cells. *J. Am. Chem. Soc.* **2011**, *133*, 11030–11033. [[CrossRef](#)]
67. Li, X.; Gao, X.; Shi, W.; Ma, H. Design strategies for water-soluble small molecular chromogenic and fluorogenic probes. *Chem. Rev.* **2014**, *114*, 590–659. [[CrossRef](#)]
68. Kumar, R.; Shin, W.S.; Sunwoo, K.; Kim, W.Y.; Koo, S.; Bhuniya, S.; Kim, J.S. Small conjugate-based theranostic agents: An encouraging approach for cancer therapy. *Chem. Soc. Rev.* **2015**, *44*, 6670–6683. [[CrossRef](#)]
69. Dujols, V.; Ford, F.; Czarnik, A.W. A Long-Wavelength Fluorescent Chemodosimeter Selective for Cu(II) Ion in Water. *J. Am. Chem. Soc.* **1997**, *119*, 7386–7387. [[CrossRef](#)]
70. Niu, G.; Zhang, P.; Liu, W.; Wang, M.; Zhang, H.; Wu, J.; Zhang, L.; Wang, P. Near-Infrared Probe Based on Rhodamine Derivative for Highly Sensitive and Selective Lysosomal pH Tracking. *Anal. Chem.* **2017**, *89*, 1922–1929. [[CrossRef](#)]
71. Wu, D.; Ryu, J.C.; Chung, Y.W.; Lee, D.; Ryu, J.H.; Yoon, J.H.; Yoon, J. A Far-Red-Emitting Fluorescence Probe for Sensitive and Selective Detection of Peroxynitrite in Live Cells and Tissues. *Anal. Chem.* **2017**, *89*, 10924–10931. [[CrossRef](#)] [[PubMed](#)]
72. Kubin, R.F.; Fletcher, A.N. Fluorescence quantum yields of some rhodamine dyes. *J. Lumin.* **1982**, *27*, 455–462. [[CrossRef](#)]
73. Kim, H.N.; Lee, M.H.; Kim, H.J.; Kim, J.S.; Yoon, J. A new trend in rhodamine-based chemosensors: Application of spirolactam ring-opening to sensing ions. *Chem. Soc. Rev.* **2008**, *37*, 1465–1472. [[CrossRef](#)] [[PubMed](#)]
74. Beija, M.; Afonso, C.A.; Martinho, J.M. Synthesis and applications of Rhodamine derivatives as fluorescent probes. *Chem. Soc. Rev.* **2009**, *38*, 2410–2433. [[CrossRef](#)]
75. Chen, X.; Pradhan, T.; Wang, F.; Kim, J.S.; Yoon, J. Fluorescent chemosensors based on spiroring-opening of xanthenes and related derivatives. *Chem. Rev.* **2012**, *112*, 1910–1956. [[CrossRef](#)]
76. Gong, Y.J.; Zhang, X.B.; Mao, G.J.; Su, L.; Meng, H.M.; Tan, W.; Feng, S.; Zhang, G. A unique approach toward near-infrared fluorescent probes for bioimaging with remarkably enhanced contrast. *Chem. Sci.* **2016**, *7*, 2275–2285. [[CrossRef](#)]
77. Song, Z.J.; Ng, M.Y.; Lee, Z.W.; Dai, W.; Hagen, T.; Moore, P.K.; Huang, D.; Deng, L.W.; Tan, C.H. Hydrogen sulfide donors in research and drug development. *Med. Chem. Commun.* **2014**, *5*, 557–570. [[CrossRef](#)]

Sample Availability: Samples of the compounds **1** are available from the authors.



© 2020 by the authors. Licensee MDPI, Basel, Switzerland. This article is an open access article distributed under the terms and conditions of the Creative Commons Attribution (CC BY) license (<http://creativecommons.org/licenses/by/4.0/>).